ADVANCED ENGINEERING MATERIALS
www.aem-journal.com

A Positron Lifetime Study of Cooling and Natural Aging of Solutionized Aluminum Alloys

*Zi Yang, Mengjie Li, and John Banhart**

Fast cooling of aluminum alloys from the solutionizing temperature to "room temperature," during which solute atoms and vacancies evolve rapidly, is the step defining all ensuing age-hardening treatments. Six Al–Mg and Al–Mg–Si alloys are solutionized and air-cooled at a moderate rate, after which cooling is interrupted in various stages by fast quenching and positron lifetime measured at 20 °C. In the ternary alloys, two main processes during cooling are found, continuous vacancy loss followed by solute cluster formation, whereas in the binary alloy, the latter process is absent. The extent of clustering is higher for high solute content, especially Si, while Sn addition to the alloy delays it. Compared to analogous calorimetry and resistivity measurements, positron lifetime measurement shows a unique sensitivity to vacancy evolution and an enhanced sensitivity to solute clustering.

1. Introduction

Accelerated cooling is a critical step after the solution heat treatment of age-hardenable aluminum alloys and aims at preserving a level of supersaturation of solute atoms sufficient to sustain the precipitate formation in the subsequent aging step. Besides solutes, many thermal vacancies are also frozen in, usually at a concentration level much higher than the thermal equilibrium at the end temperature. These excess vacancies enhance solute diffusion and accelerate precipitate formation, especially at low temperatures such as "room temperature" (RT), a phenomenon well-known as natural aging (NA). NA is found in the full spectrum of age-hardenable aluminum alloys but receives particular attention in 6xxx (Al–Mg–Si based) alloys due to its detrimental impact on the subsequent artificial aging. Therefore, it is the objective of the current work to investigate the evolution of vacancies during cooling and their influence on the following NA clustering in various 6xxx alloys.

Positrons can be utilized to probe a material's microstructure and reveal information that are sometimes "hidden" to other characterization techniques. For example, the lifetimes of positrons can inform on the local electron densities of their annihilation sites, thus allowing us to distinguish between various microstructural features such as the bulk matrix lattice, vacancies, solutes, and/or their clusters. The technique, the so-called positron annihilation lifetime spectroscopy, has been applied to study precipitation in a variety of alloys (for example, steels,[1,2] Cu,[3] Ni-Ti,[4] Al, and Mg alloys[5]) and has been especially successful in revealing the evolution of vacancies and solute clusters at early stages of aging.[5–8] In a prior study, the present authors utilized this method to investigate the impact of different quenching strategies on NA kinetics of a 6xxx series aluminum alloy.[9] A vacancy concentration difference of about 1 to 2 orders of magnitude was revealed when different cooling pathways were applied, and an intriguing "kinetic compression effect" was noticed, meaning that such a large discrepancy does not translate to an overall difference of clustering kinetics. This suggests that complex interactions between vacancies and solute clusters take place in the early stage of NA and significantly influence the following processes. In this work, we extend such positron lifetime (PLT) studies to further alloys in which the solute/cluster–vacancy interactions are altered. This includes 1) alloys with different Mg and Si contents which demonstrate different cluster formation rates and thus retrointeraction on the vacancies, 2) Sn-added alloys, in which an external vacancy-interacting force is exerted, and 3) a binary Al–Mg alloy, which serves as a reference system as it does not contain MgSi clusters that can affect vacancy evolution and obscure the PLT analysis. Initial vacancy concentrations are varied by performing cooling at 5 K s^{-1} (on average) followed by fast quenching after reaching one of the predefined temperatures. Through comprehensive analyses of all these alloys and their respective states, we aim to deepen our understanding of vacancy evolution during cooling and the subsequent solute clustering processes occurring during NA.

2. Experimental Section

The six alloys investigated were provided by Novelis Switzerland or by Hydro Aluminium Bonn (now Speira GmbH), Germany, as

Z. Yang, M. Li,[+] J. Banhart
Department of Microstructure and Residual Stress Analysis
Helmholtz-Zentrum Berlin für Materialien und Energie GmbH
Hahn-Meitner-Platz 1, 14109 Berlin, Germany
E-mail: banhart@helmholtz-berlin.de, john.banhart@tu-berlin.de

The ORCID identification number(s) for the author(s) of this article can be found under https://doi.org/10.1002/adem.202501999.

[+]Present address: Leibniz-Institute for Solid State and Materials Research (IFW), Helmholtzstraße 20, 01069 Dresden, Germany

DOI: 10.1002/adem.202501999

Table 1. Alloys investigated. Compositions (given in at.% and wt%) measured by optical emission spectroscopy. Code in column "origin": N for Novelis Sierre, Switzerland, and H for Hydro Aluminium Bonn, Germany.

Alloy code	Mg	Si	Sn	Other elements	Origin
AlMg1	1 at.%	Impurities	–	<10 wt.ppm	H
4-4	0.39 wt% 0.43 at.%	0.40 wt% 0.38 at.%	–	<10 wt.ppm	H
4-4-Sn	0.4 wt% 0.45 at.%	0.41 wt% 0.40 at.%	200 wt.ppm 45 at.ppm	Cu: <100 wt.ppm	N
6-8	0.59 wt% 0.66 at.%	0.79 wt% 0.76 at.%	–	<10 wt.ppm	H
6-8-Sn	0.6 wt% 0.67 at.%	0.80 wt% 0.77 at.%	180 wt.ppm 41 at.ppm	Cu: <100 wt.ppm	N
6014	0.65 wt% 0.72 at.%	0.60 wt% 0.58 at.%	–	0.18 wt% Fe, 0.08 wt% Mn, 0.12 wt% Cu	N

sheets of 1 mm thickness. Their compositions are given in **Table 1**.

Samples were cut into pieces of $\approx 10 \times 10 \times 1\,\text{mm}^3$ size and solutionized at about 540 °C for 1 h in an air circulation furnace before being cooled in resting air. The temperature of the sample was monitored during cooling; for details, see ref. [9]. The average cooling rate in the range 533–250 °C was $\approx 5\,\text{K s}^{-1}$, and the initial cooling rate was $\approx 8\,\text{K s}^{-1}$. After a predefined interruption temperature T_i had been reached during cooling, the sample was quenched in ice water. This causes rapid transfer to near 0 °C at rates around $1000\,\text{K s}^{-1}$, and therefore, the state reached after cooling to the predefined temperature T_i is largely conserved. **Figure 1**a visualizes the procedure, and Figure 1b shows measured sample temperature courses. We shall use the word *quenching* only for the latter fast ice water quenching and the word *cooling* for the primary air cooling in this article.

NA was performed in an air-conditioned room at 20 ± 2 °C while measuring PLT spectra continuously using a fast–fast coincidence system. Positrons were produced by a ^{22}Na source of activity ≈20 μCi enveloped in Kapton foil, which was sandwiched by two identically processed alloy samples during measurement. The spectrometer had a resolution (full width at half maximum) of ≈220 ps and a count rate of $\approx 400\,\text{s}^{-1}$ due to the use of a strong source and efficient plastic scintillators. Such high count rate allows one to determine the PLT in a one-component spectrum such as in most Al-Mg-Si alloys in just a few minutes.[10] Spectra were recorded in intervals of 2 min and stored. Such short intervals allow us to bin a given number of adjacent spectra after measurement whenever necessary. For aging times longer than 100 min, spectra were binned progressively to produce approximately equidistant data on the logarithmic time scale, but for shorter aging times, various binning options were applied to find the most favorable combination of temporal resolution and reduced noise in the PLT curve over NA time. This will be further discussed in Section 3.2.

Before further analysis, PLT spectra had to be processed, which was done with program LT9 that allows for convenient batch processing of the large number of spectra. First, a reference spectrum was measured on a pair of 5 N-pure soft-annealed Al samples with a known one-component PLT of ≈160 ps. This measurement yielded the positron decay components caused by the source itself and by the Kapton foil. It also allows to determine the spectrometer resolution function. Then, the alloy spectra were corrected for source and Kapton contributions, background and spectrometer resolution. In Al–Mg–Si alloys, a one-component lifetime τ_{1C} was sufficient to represent the spectra. For the binary alloy AlMg1, spectra could be decomposed into two individual components τ_1 and τ_2 after extending binning to over 60 min, thus gathering more data.

The delay between quenching and the start of the measurements was around 2 min. This implies that the first value for τ_{1C} is obtained just a few (minimum 3) minutes after quenching. Moreover, the measured τ_{1C} was found to evolve during NA. Therefore, to determine the PLT τ_{1C}^0 corresponding to the state directly after quenching (green circle in Figure 1a), a back-extrapolation procedure based on the measured data during NA (green disks in Figure 1a) is needed (see Section 3.2).

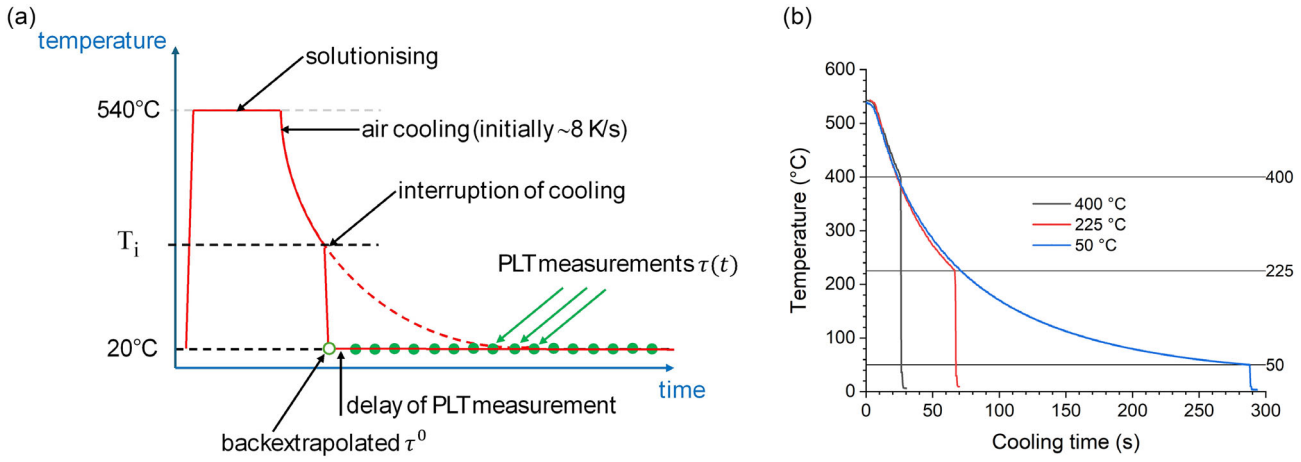

Figure 1. a) Schematic of measurements. b) Exemplary experimental cooling curves.

Transmission electron microscopy (TEM) was conducted on alloy 6014 after air cooling down to RT for the observation of the interspacing between the precipitate/dispersoid particles. It was performed on a Philips CM30 unit operated at 300 kV with samples prepared via twin-jet electropolishing in an electrolyte mixture of 75% methanol and 25% nitric acid at −20 °C. Observation was done along the ⟨100⟩ directions of the surrounding matrix. The integrated energy-dispersive X-ray detector of the CM30 was used to determine elemental compositions.

3. Results

3.1. NA

Figure 2 shows the results for all six measured alloys. Measured PLTs τ_{1C} are seen to evolve during NA after solutionizing at 540 °C, air cooling to an interruption temperature T_i, and fast quenching. Some measurements were stopped after 2 h as their trends can be expected from the courses of the other curves.

The binary AlMg1 alloy, Figure 2a, shows a slow decrease of $\tau_{1C}(t)$ during NA for all of the nine interruption temperatures T_i applied and for the sample directly quenched from 540 °C. The initial value is highest for direct quenching from 540 °C and decreases monotonically for lower T_i and reaches 165 ps when air cooling takes place down to 25 °C.

Alloy 6014 shows a behavior different from AlMg1 (see Figure 2b). The highest T_i (533 °C) gives rise to an initial PLT slightly lower than in AlMg1. With lower T_i, the initial value also decreases and reaches a minimum for $T_i = 192$ °C, after which it increases again to reach 220 ps for air cooling down to 21 °C. During NA, PLT evolves markedly unlike in AlMg1. For direct quenching from the solutionizing temperature ($T_i = 533$ °C), we obtain the typical curve already discussed in other papers, namely, an initial rather constant stage I, followed by a decrease (stage II), reincrease (stage III), and final decrease (stage IV), with definition of stages in ref. [10]. As T_i is lowered, the first stage begins to show an increase in PLT up to 225 ps, followed by an ordinary decreasing stage II. All curves roughly merge into one curve after 100 min of NA and then reach ≈218 ps (see lines and circle in graph), after which they further increase to a maximum at 220 ps after 1000 min of NA and decrease slightly after. As the initial PLT for high T_i is above 222 ps, we observe an initial PLT decrease, whereas for initially low PLT, there is an increase.

Alloy 4-4 shows a similar trend in PLT as alloy 6014 when it is quenched from the solutionizing temperature ($T_i = 540$ °C) (see Figure 2c). However, as T_i is lowered, a pronounced distinction can be seen. Positron lifetimes approach the end of stage II monotonously either from higher initial values ($T_i > 298$ °C) or from lower initial values ($T_i < 298$ °C). In other words, there is no increase of PLT to a level as high as ≈225 ps and an associated PLT maximum anymore. Why this is a matter of interest will be further discussed later in this article.

The addition of Sn to alloy 4-4 markedly modifies the course of NA (Figure 2d). In analogy to the Sn-free alloy, the initial values of τ_{1C} decrease with decreasing T_i, reach a minimum, but then increase only slightly. The course during NA is greatly decelerated compared to the Sn-free alloy. Within the measurement time in this work, only one stage is visible, but a longer measurement shows that full stages can be observed as in the Sn-free alloy.[11] However, all the processes take much longer. For example, the curve for $T_i = 540$°C in Figure 2c features a decrease to 220 ps in just 50 min in the Sn-free alloy, whereas in the corresponding Sn-containing alloy, we observe that the same lifetime is reached only after 4000 min, in other words, delayed by a factor of 80. Similarly, for the curves representing $T_i = 247/248$ °C, such factor is 150 when measuring the time of increase to 200 ps. Thus, there is a general aging delay of kinetics by about ≈100 times in alloy 4-4 with Sn.

The alloy with a higher Mg and Si content (6-8) shows a behavior similar to alloy 6014, but is kinetically much faster. Here, the end of stage II is observed after NA for 30 min. An increasing stage I also takes place in the first 10 min, but as it happens really fast, it is only captured when using lower time binning of the spectra (see Figure 2h).

The Sn-containing counterpart of the alloy, 6-8-Sn, exhibits a clearly distinguishable stage I for about 60 min, then a decrease (stage II), and reincrease (stage III) (Figure 2f). The evolution during even longer NA has been reported in ref. [11]. Figure 2g presents such comparisons for $T_i = 540$ and 200 °C, where a factor of ≈10 can be derived from the delay in NA kinetics by adding Sn in alloy 6-8. The very short initial increase of PLT in stage I of the $T_i = 200$ °C sample of alloy 6-8, which consists of only two data points, is now very obvious in 6-8-Sn and extends over 100 min.

3.2. Back-Extrapolation to Zero NA Time

To obtain the values of the PLT directly after quenching, $\tau_{1C}^0(T_i)$, the time-dependent data in Figure 2 are extrapolated back to zero NA time for all six alloys investigated. To avoid any accidental bias induced by the choice of the binning parameters (Figure 2h shows four choices), for each alloy and T_i, we first analyzed the PLT curve using different time binnings from 2 to 8 min (Figure 2a–g shows such curves with a binning of 6 min). For each such binning option, we applied weighted linear regression to the first several data points (including errors) within a given NA time, which is 16 min for all the alloys except for alloy 6-8, where we use 8 min due to the very rapid progress in the initial stage. Average and standard deviation were subsequently taken from the intercepts of the fittings with different time binnings, representing each point in **Figure 3**. In this way, we also handle the error propagation rigorously from the PLT spectra fitting to linear regression and to averaging. It is seen that except for alloy 6-8, all other alloys are not very sensitive to the binning parameters, thus smaller error bars. The longer error bars for alloy 6-8 are caused by the rapid evolution of PLTs during early NA. The curve for alloy 6014 had already been discussed in ref. [9], but now, the curve is supported by more values of T_i.

The first value corresponding to direct quenching from 540 °C is higher for alloy 4-4 than for alloys 6-8 and 6014 in accordance with.[7,10] For both 4-4 and 6-8, Sn slightly reduces the first value.

All ternary alloys exhibit a decrease down to a minimum at between 220 and 180 °C and a reincrease after. Only in the binary alloy, $\tau_{1C}^0(T_i)$ decreases monotonically. The PLT at the minimum differs: It is highest for alloy 6-8, and lower for 4-4 and 6014, whereas for the binary alloy, the values go down to 163 ps. Sn

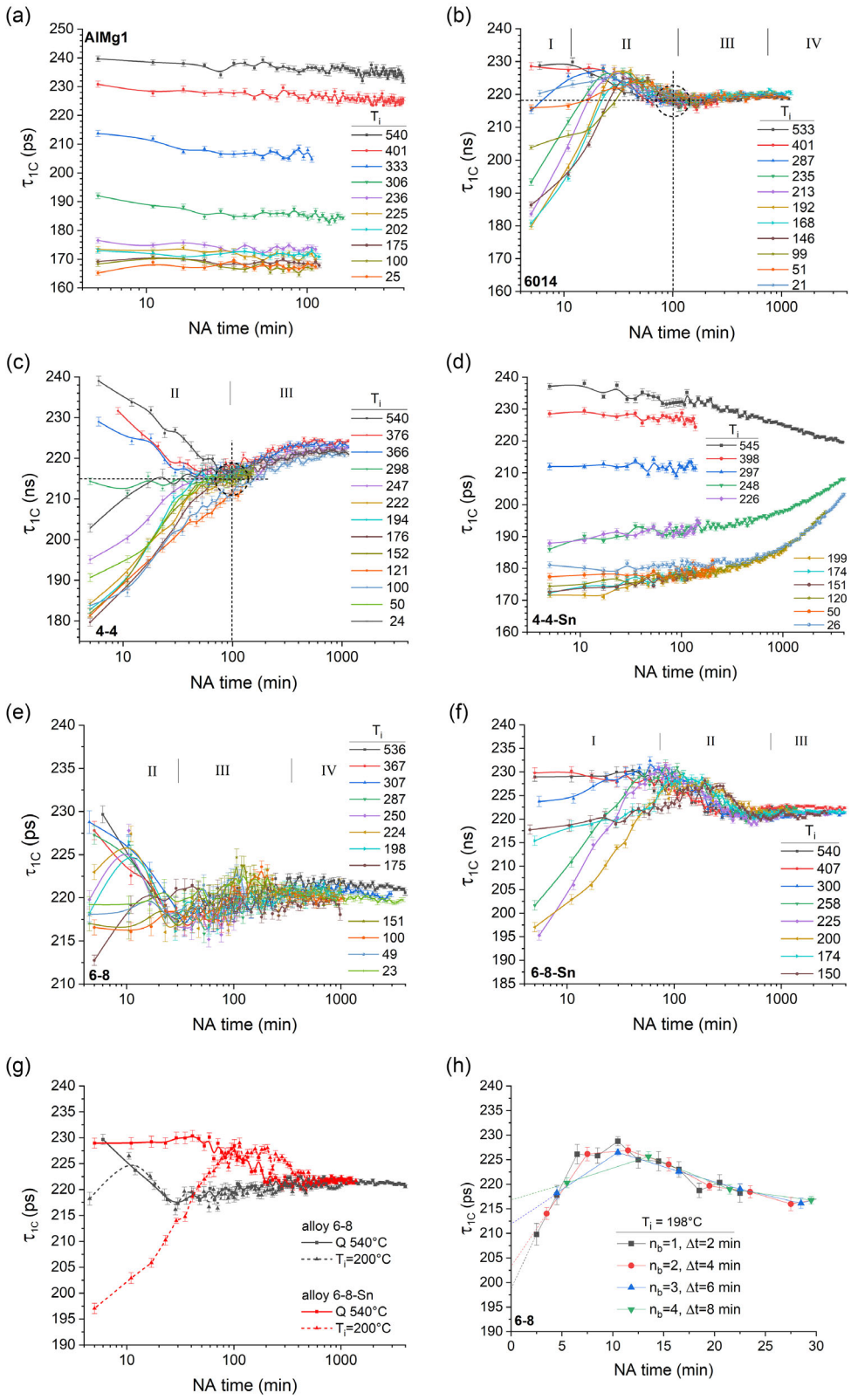

Figure 2. PLT during NA after cooling from 540 °C to a given T_i as given by legend and interrupting the cooling process by water quenching. a) AlMg1, b) 6014, c) 4-4, d) 4-4-Sn, e) 6-8 f) 6-8-Sn, and g) comparison between 6-8 and 6-8-Sn. Each data point in (a–g) represents 6 min of spectra acquisition. h) Comparison of various binning options for alloy 6-8, n_b is the number of adjacent spectra added up to one, only first 30 min of NA. $T_i = 198$ °C. Time axis is linear unlike in (a–g).

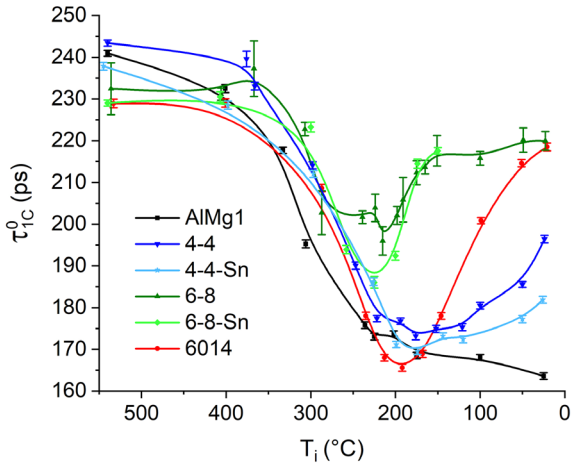

Figure 3. PLT $\tau^0_{1C}(T_i)$ of six alloys back-extrapolated to zero NA time, representing the postquenching state. The error bars represent a combination of fitting errors of PLT lifetime deconvolution with the scatter of extrapolations caused by different binnings of positron data.

addition to both 6-8 and 4-4 reduces the minimum value. The minimum occurs at higher temperatures for the 6-8 and 6-8-Sn alloys, at lower temperatures for alloys 4-4 and alloy 4-4-Sn, while the lowest is alloy 6014.

The magnitude of the PLT increase below the minimum depends on the alloy: The concentrated alloys 6-8, 6-8 Sn, and 6014 show the highest increase with final values around 220 ps. Alloys 4-4 and 4-4 Sn increase less, the former reaches 200 ps, and Sn further reduces this value. Therefore, Sn addition slows down the reincrease predominantly in 4-4 alloy but to a much less extent in 6-8 alloy.

4. Discussion

We shall first explain the general interpretation of PLT in Al–Mg–Si alloys, give a preview on what one might expect via calculations, and then first discuss the state after cooling and quenching, after which the entire course of PLT during NA is discussed.

4.1. General Interpretation of Positron Lifetimes

The PLT in a system such as an aluminum alloy is given by a superposition of various possible contributions. As positron spectra can be decomposed into various components only in special cases, we usually have to discuss the average of all contributions and interpret changes of the average in terms of changes of one or more individual components based on plausibility considerations.

In previous discussions of PLT in naturally aged Al–Mg–Si alloys, it has been assumed that positrons annihilate either in the bulk (defect-free lattice) without being trapped and have a (reduced) lifetime $\tau_1 \leq 160$ ps there, or they are trapped in single (1V) or multiple vacancies (nV) and have a lifetime of $\tau_3 = 245$ ps (1V) or higher, or they are trapped in vacancy-free solute clusters or coherent precipitates, where the typical PLT τ_2 is estimated to be between 210 and 220 ps depending on the composition.[8] Vacancy clusters give rise to higher PLTs (see Appendix A.1).

The measured average PLT is given by the relative intensities of each of the three (or possibly more) contributions

$$\overline{\tau} = I_1\tau_1 + I_2\tau_2 + I_3\tau_3, \text{with } I_1 + I_2 + I_3 = 1 \quad (1)$$

Based on these three assumptions, any change of average PLT during aging can be interpreted as being caused by a change of the intensity of individual components as given in **Table 2** where B, V, C stand for bulk, vacancy, and cluster. As vacancies can only be lost during isothermal aging, there is no "+V".

In this context, we have neglected annihilation at grain boundaries and dislocations due to their low number density, and that clusters might have a range of different sizes and compositions (which in turn would lead to a range of PLTs). We also neglect that the PLT in vacancies is modified by neighboring atoms. Enrichment in Mg, for example, is thought to increase PLT ("+Mg" in Table 2).[10] Currently, there is no way to measure such PLT variations directly. Finally, the formation of divacancies from individual vacancies might also increase PLT (+D). We explain this nontrivial fact in Appendix A.1.

Whenever $\overline{\tau}$ cannot be determined due to insufficient statistics of the short data sets collected during NA and corresponding unreliable two-component decompositions, the one-component lifetime τ_{1C} is used to characterize NA (see Figure 2). τ_{1C} contains almost the same information as $\overline{\tau}$. However, there can be a gap between τ_{1C} and $\overline{\tau}$ as discussed previously (online supplement to ref. [12] and supplement S4 to ref. [11]). Relying on one-component fits is justified in cases where trapping is predominantly (or exclusively) in one trap, for example, in clusters of a high number density and when the trapping is strong enough to prohibit bulk annihilation. Sometimes, however, two mechanisms with different lifetime components contribute to a positron spectrum but still cannot be deconvoluted with certainty due to a too low number of recorded annihilation events as in our in situ measurements. This leads to an increased fitting error of the positron spectra and τ_{1C} might deviate from the true

Table 2. Alternative mechanisms governing the change of the averaged ($\overline{\tau}$) or one-component PLT (τ_{1C}) during isothermal aging of Al–Mg–Si alloy. "+" and "−" denote an increase or decrease of a specific contribution. In this article, vacancy (V) loss, clustering (C), the change of bulk annihilation (B), change of Mg content (Mg), and di(multi)vacancy formation (+D) are addressed. Adapted from ref. [12].

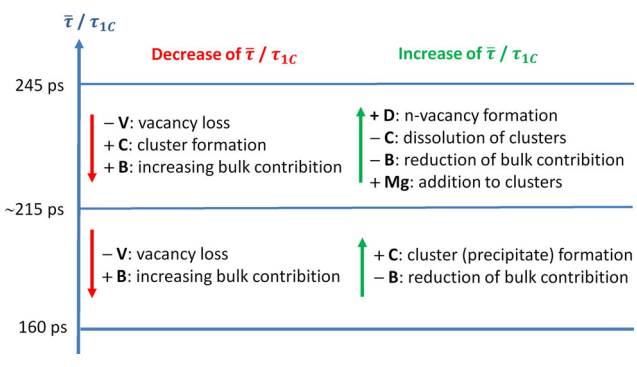

average of two components $\overline{\tau}$. We have found empirically that this is especially the case directly after solutionizing and quenching and that $\tau_{1C} > \overline{\tau}$ there with a difference up to 14 ps (see simulation in the Appendix A.2). This is also the case in Figure 2a for the high interruption temperatures.

4.2. Calculations of PLT due to Vacancy Evolution

Before we interpret the experimental PLT curves containing multiple positron annihilation components, we can first simulate how pure vacancy evolution during quenching and NA would influence the PLT evolution. To that end, we use the FSAK model of vacancy dynamics[13] to calculate the vacancy site fraction during the experiment, including cooling from 540 °C to a given T_i—represented by the experimental cooling profile—the following fast quenching, assuming a linear decrease at $-1000\,\mathrm{K\,s^{-1}}$ down to 20 °C, and NA at 20 °C. **Figure 4**a specifies the corresponding temperature profiles. Vacancy annihilation exclusively in dislocation jogs was assumed (dislocation density $10^{11}\,\mathrm{m^{-2}}$, one jog every 50 atoms). The simple trapping model[14] is used to calculate the average PLT using the trapping coefficient in a vacancy of $\mu_v = 2.5 \times 10^{14}\,\mathrm{s^{-1}}$[15] (see also Appendix A.1)

$$\overline{\tau} = \tau_B \frac{1 + x_v \mu_v \tau_v}{1 + x_v \mu_v \tau_B} \tag{2}$$

where x_v is the site fraction of the vacancies and τ_B and τ_v the bulk and vacancy PLTs, respectively.

Figure 4b shows the course of $\overline{\tau}$ for the different interruption temperatures T_i in pure Al. We start at 231 ps during solutionizing (A). Air cooling down to 20 °C (purple line) leads to a decrease down to 160.4 ps. This is very close to pure bulk annihilation, i.e., many vacancies have been annealed out. The curve is slightly shifted to the right compared to the equilibrium state (broken line), showing that during air cooling, some vacancy supersaturation is preserved. The small size of the shift may create the impression that the supersaturation is negligible, but this is due to the low sensitivity of PLT to vacancy site fraction whenever

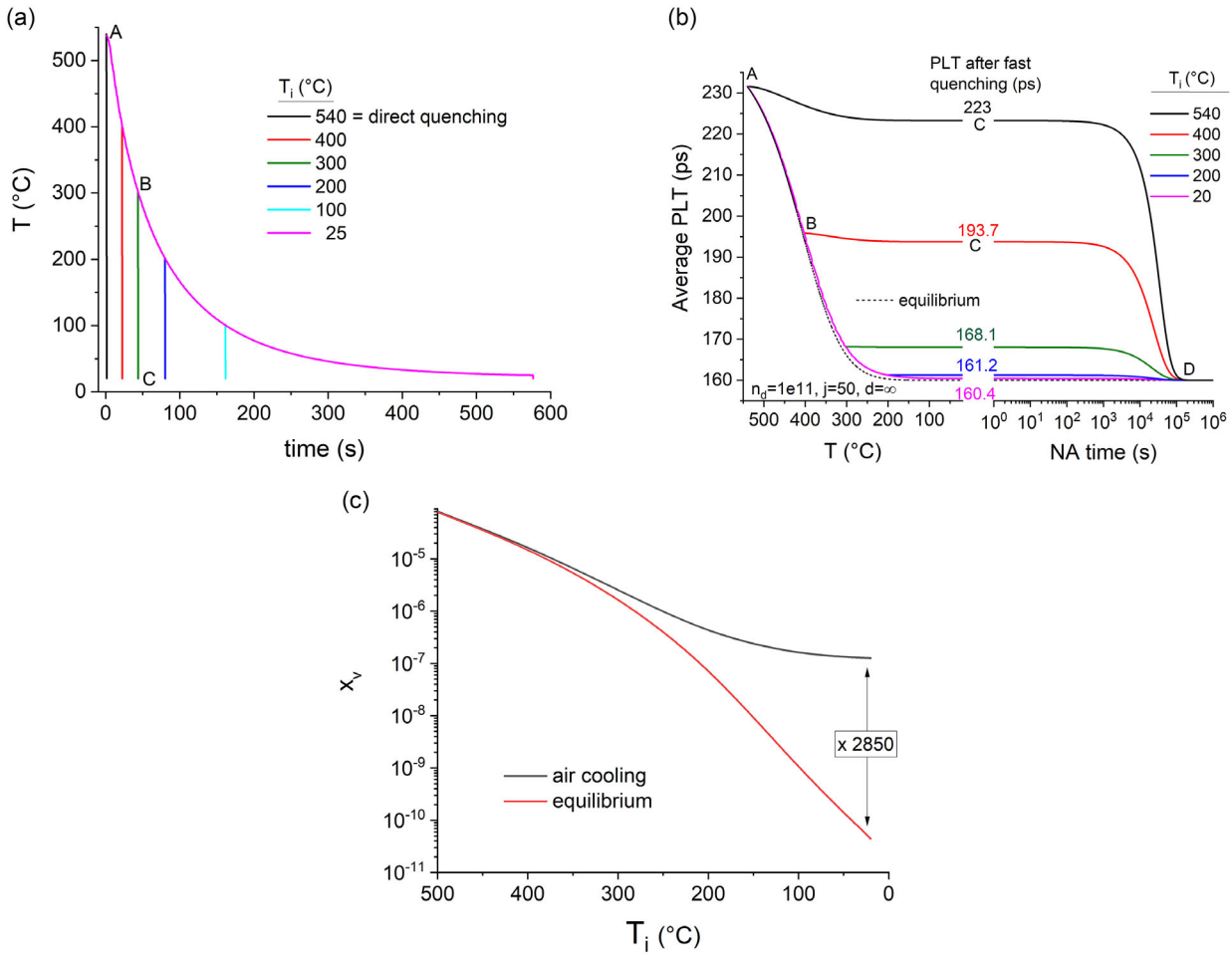

Figure 4. Calculations of vacancy site fraction occurring in various experiments. a) Temperature profiles assumed for calculation. Black: direct fast quenching from 540 to 20 °C, other colors: first cooling at the rate given by the experiment and then interruption by fast quenching after reaching given temperatures T_i. b) Calculated average PLT during the entire cooling/quenching process and, in addition to (a), ensuing NA in pure Al. The PLT corresponding to the equilibrium vacancy site fraction is also given as a broken line. The letters A to D denote various stages; curve for 100 °C that lies between 200 and 20 °C has been omitted. c) Comparison of vacancy site fraction x_v during air cooling and in equilibrium.

$\overline{\tau}$ is close to 160 ps (see Appendix A.3). Figure 4c shows the simulated vacancy site fraction throughout air quenching, and a supersaturation of almost 3000 is maintained at 20 °C.

Interrupting cooling at 200 °C yields almost the same result with a final PLT of 161.2 ps, but as the interruption temperature increases, the final PLT also does. During direct quenching from 540 °C, a decrease of 8 ps is observed.

During the interruptions of air cooling by fast quenching, the decreases of PLT are small. Therefore, it is justified to take the values after fast quenching (marked "C" in Figure 4b) as a measure for the state at the end of air quenching (marked "B"). This is the rationale for the experiment in this article: We can follow the evolution of PLT in a dynamic state (here during cooling) by measuring PLT after interruption through fast quenching.

During ensuing NA, the PLT steadily decreases to 160 ps, state "D" in Figure 4b, as vacancies continue to diffuse out of the Al matrix, the time of which depends on the vacancy sink density. This time is just of the order 10^5 s here. We know that in AlMg1, the PLT does not decrease to 160 ps in such a short time (see Figure 2a, longer aging times are documented in ref. [16]). One reported measurement even shows a PLT of still 190 ps after 1 year of NA in a AlMg0.5 alloy.[17] The reason is the stabilization of vacancies via formation of vacancy–Mg (multi)complexes as discussed in refs. [16,17] that are not accounted for in this calculation. Moreover, the FSAK model has been shown to overestimate the loss of vacancies during quenching in many cases.[18] The decrease of PLT as given in Figure 4b might therefore be much slower in reality.

4.3. Back-Extrapolated Positron Lifetime

4.3.1. Vacancy Evolution during Cooling

The experimental back-extrapolated PLTs shown in Figure 3 demonstrate clear two-stage behaviors except for alloy AlMg1, where the PLT monotonously decreases from values above 225 to 165 ps as the interruption temperature T_i goes from 540 to 25 °C. Such behavior is very well represented by the calculations in the previous section, Figure 4b, namely, that the decreasing PLT reflects the decreasing vacancy site fraction during air cooling.

Only for AlMg1, the spectra can be decomposed into two components if we bin all the spectra obtained in the first 60 min. This is permitted since the one-component lifetime is almost constant, and the slight slope is expected not to produce a high deviation. We obtain an average of the two components that can be identified as $\overline{\tau}^0(T_i)$, the value after interruption of quenching, and compare it to $\tau_{1C}^0(T_i)$ in **Figure 5**. We note a difference at all $T_i \geq 300$ °C and $\overline{\tau}^0(T_i) \leq \tau_{1C}^0(T_i)$ in line with the comments in Appendix A.2.

The two-component data is also used to quantify the vacancy site fraction using the standard trapping model (see Figure 5). We obtain a monotonous decrease from almost 10^{-4} for direct quenching to 1.3×10^{-6} for air cooling down to 25 °C. The upper value coincides with the calculation (see Figure 4c), whereas the lower is about seven times higher. This could be the influence of Mg atoms that delay vacancy loss at low temperatures. Thus, during air cooling, the majority of excess vacancies are annealed out. As the Al–Mg–Si alloys all follow a similar trend of decrease in the first stage down to certain temperatures, it can be assumed that a pronounced loss of thermal vacancies also exists in those alloys.

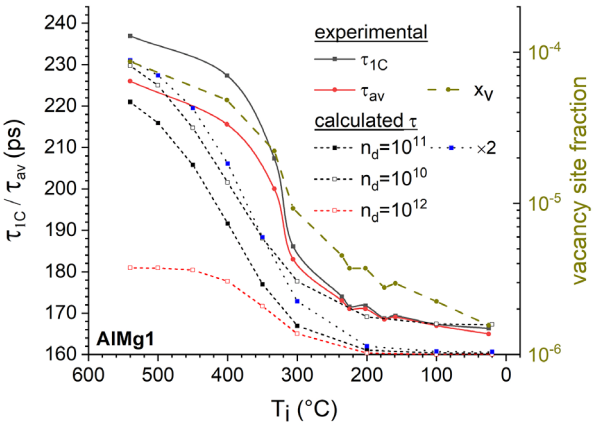

Figure 5. PLT in AlMg1 alloy after solutionizing and air cooling to T_i interrupted by rapid quenching. Values were back-extrapolated to zero NSA time. Calculated values are taken from Figure 4b (numbers on r.h.s.).

A comparison between the calculations and the experimental PLT evolution, however, reveals two noteworthy features: 1) The final measured value of 165 ps reached at "RT" is higher than the value of 160 ps expected for predominant annihilation in the bulk (as measured on a pure high-purity Al sample). 2) The measured decrease of PLT at high temperatures is too slow from what one expects from the calculations. This is even more pronounced for the other five alloys investigated (see Figure 3).

1) It is implied that even after slow cooling down to 25 °C, there are still more positron trapping centers in the material than expected (2×10^{-7} according to Figure 4c), including 1D or 2D defects. Moreover, although the alloy is in the single-phase region at all temperatures,[19] the formation of Mg_nV_m complexes with binding energies higher than the single Mg–V binding has been postulated.[17] Possibly, this leads to the binding of excess vacancies and to the slightly higher observed value of PLT. Finally, analog PALS spectrometers show uncertainty in absolute calibration, which could also contribute to a few ps of PLT.

The second deviation 2) can have various origins. First, vacancy losses during fast quenching, from A to B in Figure 4b, are larger for higher interruption temperatures T_i due to faster vacancy diffusion to sinks, which makes the curve flatter. Second, even in situ measurements of PLT in pure Al at various temperatures exhibit a flattening of $\overline{\tau}$ above 480 °C (Figure 2 of ref. [15]), and another source shows almost constant τ above 500 °C (Figure 1 of ref. [20]), which resemble the flat curves in Figure 3 and 5. Ref. [15,21] explain the effect by saturated positron trapping, but it is not quite clear why this would already happen at vacancy site fractions around 10^{-4}.

The FSAK calculations contain the dislocation density and jog spacing as parameters. These values are not precisely known. The parameters used ($n_d = 10^{11}$ m^{-2} and 50, respectively) are motivated by considerations in ref. [13] rather than having been exactly determined. We therefore show results based on two other values of n_d in Figure 5. A ten times higher n_d leads to much faster vacancy annihilation and correspondingly very

low PLTs. A ten times lower n_d increases PLTs but still does not explain the initial flat stage. Moreover, a possibly higher value (twice as high as given by ref. [15]) of the positron trapping coefficient μ is evaluated, but none of these variants explain the flat stage. Flat curves at high temperatures would also be observed if the site fraction of vacancy annihilation sites (mostly dislocation jogs) was initially low but increased at lower temperatures, say below 400 °C. This was already speculated in previous work,[12] but the possible mechanism remains elusive. In summary, the exact reason for the flat curves is not totally clear.

4.3.2. Precipitation and Cluster Formation during Cooling

In ternary Al–Mg–Si alloys, precipitation processes are known to take place during cooling unless a critical cooling rate is exceeded. Continuous cooling precipitation (CCP) diagrams have been measured by differential scanning calorimetry (DSC) during the cooling of various alloys from the solutionizing temperature.[22] Two of the alloys investigated there are similar to the alloys in this study, namely 6060 alloy which is close to our alloy 4-4 and "6082_{low}" alloy, which is close to alloy 6-8. To a lesser extent, 6014 can be compared to alloy 6005A.

The DSC study reveals that during air cooling of alloy 4-4 (applying the temperature profile given in Figure 1b to the CCP diagrams in ref. [22]), no reactions take place whenever cooling is faster than a critical rate of 30 K min^{-1} (0.5 K s^{-1}). This is much slower than the rate applied in this study in the temperature range where precipitation is strongest (above 250 °C). In contrast, in alloy 6-8, a field of metastable phase formation associated to β′ or B′ is crossed from about 350 °C down to 240 °C at the cooling profile applied here. The reason is that the critical cooling rate is 1000 K min^{-1} in that alloy (16.7 K s^{-1}), which is much higher that the cooling rate we apply. Alloy 6005A finally lies between the two alloys 6060 and 6082_{low} and exhibits a critical cooling rate of 375 K min^{-1} (6.25 K s^{-1}), which is slightly above the rate applied in this study in the region of precipitation.

In the cooling regime around 300 °C, however, all the 5 Al–Mg–Si alloys show similar PLT courses within the experimental errors. Therefore, phase formation during cooling of alloys 6-8 and 6014 around 300 °C does not lead to precipitation that can influence PLT because the precipitates are too large and sparsely distributed. This can be seen from the TEM images in **Figure 6** that were taken from a sample after air cooling to RT. The image features dislocations and coarse phases but no fine-scale precipitation in the space in between. As the diffusion length of thermalized positrons is about 100 nm,[14] most of them will annihilate far away from such coarse heterogeneities as depicted by the red circle in Figure 6a. Figure 6b gives a close-up of an intermetallic particle high in Fe, Si, and Mn at which an Al–Mg–Si precipitate has nucleated. The two types of precipitates can be easily distinguished by energy-dispersive x-ray spectroscopy (EDX) scans carried out in the TEM. Both precipitates give rise to Al and Si signals, but only the intermetallics show clear Fe and Mn signals, while the precipitates feature an additional Mg signal. Corresponding EDX spectra can be found in ref. [23]. Such precipitates are found almost exclusively attached to the coarse intermetallics and therefore do not notably influence PLT.

A second stage of PLT evolution is observed in Al–Mg–Si alloys, namely, as the interruption temperature T_i is further lowered, τ_{1C} increases again after the decrease caused by the loss of vacancies (–V). Table 2 tells us which mechanisms can increase PLT at this stage: It is the formation of clusters (+C) associated with a decrease of annihilation in the bulk (–B) beside the usually small contributions +D and +Mg. The minimum is the consequence of a balance of the two mechanisms –V and +C. Below the temperature of the minimum, cluster formation dominates.

The position and the magnitude of reincrease of τ_{1C} differ, which can be explained by the alloy compositions and their clustering potential. The three Al–Mg–Si alloys investigated differ in their solute content "Mg+Si" and in their Mg:Si ratio. We have two purely ternary model alloys, the lean alloy 4-4 (Mg + Si = 0.81 at.% and Mg:Si = 1.13) and the more

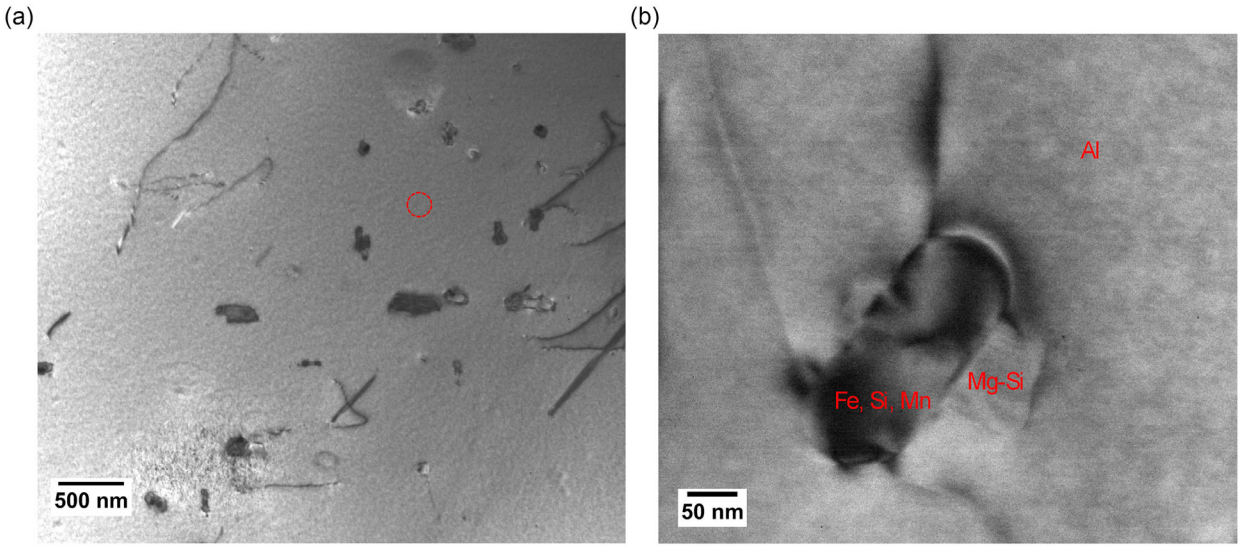

Figure 6. a) Bright-field transmission electron micrographs of 6014 sample after air cooling to RT. Red circle illustrates positron diffusion range. b) Close-up shows Al–Mg–Si phases around an intermetallic AlFeMnSi particle, both embedded in the Al-base solid solution matrix (marked "Al").

concentrated alloy 6-8 (Mg + Si = 1.41 at.% and Mg:Si = 0.87), and one engineering alloy 6014 (Mg + Si = 1.3 at.% and Mg:Si = 1.24). Alloy 6-8 is the only Si-rich alloy, whereas the others are Mg-rich. Alloy 6-8 has the fastest and strongest hardening during both artificial aging at 180 °C and NA at RT among the three alloys,[24] followed by alloy 6014 (or the chemically similar 8-6 in ref. [24]) and 4-4.[24] DSC results also feature an area of clustering peaks in such order.[16,17] Therefore, we can expect that alloy 6-8 has the strongest clustering tendency also during cooling, which explains its earliest minimum at 215 °C and the highest τ_{1C} at minimum of 195 ps. Alloys 6014 and 4-4 follow in clustering tendencies, thus showing a declining temperature of the PLT minimum and the magnitude of reincrease rate in this order. The minimum value of the 6014 alloy (168 ps) is surprisingly slightly lower than that of 4-4 (174 ps), which might be attributed to the fact that 6014 is a commercial alloy that contains more impurities and thus a higher density of intermetallic particles that provide additional sinks for vacancies at their interfaces. Therefore, the removal of excess vacancies in 6014 might be more complete than in the pure ternary 4-4 alloy.

Neither the DSC investigations of phase formation during cooling cited above[22] nor the course of electrical resistivity during cooling of a 6014 alloy[25] reveal the clustering stage from about 200 to 20 °C. On the other hand, both DSC and electrical resistivity reveal precipitation at higher temperatures, but PLT measurement does not. This underlines that PLT measurement is complementary to other methods and is valuable since it can trace minute clustering effects.

4.3.3. Effect of Sn Addition

In alloy 4-4-Sn, in comparison to the Sn-free counterpart, the effect of Sn is to slightly lower the PLT at the minimum and to limit the increase at lower temperatures approaching "RT." Sn addition to Al–Mg–Si alloys has been found to markedly delay aging especially at "RT." The reason for this behavior is the high binding energy between a vacancy and a Sn atom in the aluminum matrix of around 240 meV, much higher than vacancy binding with Si (60 meV) or Mg (10 meV).[26] The strong binding of vacancies by Sn atoms creates stable Sn-vacancy complexes at 20 °C and prevents vacancies from diffusing freely and transporting Si and Mg atoms to emerging clusters, thus delaying clustering and hence NA. These complexes are broken up at artificial aging temperatures, e.g., 170 °C, where vacancies can be released, a concept called "diffusion on demand."[27] Such temperature dependence also exists at decreasing temperatures and as we are air cooling down the samples and interrupting cooling, it is understandable that the effect of Sn is small at higher temperatures and increases with decreasing temperature T_i to a notable accumulated difference at "RT," where due to reduced solute, clustering the reincrease of PLT is limited.

For alloy 6-8-Sn, the addition of Sn hardly influences the PLT evolution during cooling in contrast to alloy 4-4 where Sn changes the course below 200 °C (diverging blue curves in Figure 3 vs. almost parallel green curves). The rate and magnitude of the reincrease in 6-8-Sn are both comparable to 6-8, only the minimum value is lower. Such weak influence can be attributed to a generally higher starting temperature of clustering in 6-8/6-8-Sn (215 °C/225 vs. 175 °C in 4-4 and 4-4-Sn), where the Sn-vacancy binding is notably weakened and has no marked influence on the kinetics of clustering of solutes, whereas in 4-4-Sn, Sn has a retarding effect on subsequent clustering. Even in this case, however, Sn does not have the potential to delay clustering as much as it does isothermally at RT, where, for example, hardening is delayed in time by two orders of magnitude.[11]

4.4. Course of PLT during NA

So far, we have only discussed the PLT change shortly after quenching aiming at back-extrapolating it to zero NA time. Now, we will discuss the entire NA process for longer times. The general kinetics of NA in Al–Mg–Si alloys have been discussed in many previous works.[10,28,29] Here, we mainly discuss the points that are new in the current work.

4.4.1. Stabilization of Vacancies in AlMg1 Alloy

Figure 2a shows that in AlMg1 alloy the PLT reached after cooling to T_i and interruption by quenching is higher than expected for bulk annihilation and reflects preservation of excess vacancies. During ensuing NA, there is a slight decrease of PLT. This indicates that at "RT," vacancies are being lost to sinks, but the rate is very small compared to pure Al[16] (Figure 4b). It is known that Mg atoms stabilize vacancies against annihilation (see comments in Section 4.2). As the binding energy Mg–V is commonly thought to be very small,[26,30–36] this origin for the stabilizing effect is not immediately clear. The formation of multivacancy/solute complexes with a higher binding energy than that of Mg–vacancy complexes has been proposed as an explanation,[16,17] which is possible only in the nonequilibrium state as the alloy remains in the single-phase region at all temperatures. In the absence of a proof, this mechanism still remains somewhat speculative.

4.4.2. Kinetics of NA in Al–Mg–Si Alloys at Various T_i

Unlike in AlMg1 alloy, the PLTs in Al–Mg–Si alloys eventually merge into the master curve of the sample quenched from solutionizing temperature regardless of T_i. Such behavior has been observed before for a lean alloy 6060.[37] The course is understandable as clusters gradually build up and more positrons annihilate in them, and as they reach a critical number/fraction, positron trapping in clusters is high enough that so-called saturated trapping is achieved, i.e., all positrons are trapped in the same kind of trap. The average PLT then no longer depends on the number of clusters but only on the characteristic PLT in such clusters, which evolves according to, for example, the chemistry or size evolution of the clusters. That all curves share approximately the same stage III (the reincrease of τ_{1C} up to about 1000 min NA time), which has been ascribed to Mg enrichment, strengthens this argument.

Still, there are several points that are not immediately clear. The first is the merging behavior difference between the different alloys. For alloy 4-4, the curves move towards 215 ps, which is the end of stage II, from either above or below this value, whereas for alloy 6014 and 6-8, an increase to above 225 ps is seen,

followed by a continuation of decrease in stage II. The reason for this lifetime peak is not obvious. Looking at Table 2, one finds that clustering can cause a PLT increase as long as PLT is low, but once the PLT reaches 225 ps or even more, this is not a plausible explanation any more, since the intrinsic PLT in clusters is believed to be more around 215 ps. Mg addition to clusters could increase PLT, but the question is, why PLT would then decrease again after a short time. Another possible mechanism that could increase PLT is the formation of double or multiple vacancies if the decrease of the total number density of positron annihilation centers can be overcompensated by the increase in the intrinsic PLT (see Appendix A.1), but why this would happen only in alloy 6-8 and not in alloy 4-4 is not clear. In fact, the absence of such behavior also in alloy AlMg1 indicates that such a stage must be related to coclustering of solute atoms. One possibility is that the clusters in the early stage of clustering do have an intrinsic lifetime higher than 215 ps other than previously thought. Such higher lifetime might be related to their structure which contains more open volume due to their structural immaturity or partial vacancies trapped inside. As clusters become more developed, relaxation within clusters would occur which gradually phases out the extra open volume and leads to a decrease of lifetime toward the end of stage II. This assumption implies that saturated trapping in clusters has already occurred before the end of stage II, which is consistent with the phenomena observed in 6014 and 6-8. Alloy 4-4 is known to have a slower clustering rate and lower number density of clusters as expressed by a much lower rate of hardening or increase of electrical resistivity,[7] which is the reason why saturated trapping in clusters might set in later and no saturated trapping in early-stage low-density clusters is observed.

A similar peak of PLT has been discovered in samples that were exposed to a short temperature pulse after solutionizing and quenching and were then naturally aged, during which PLT was measured, and it is very likely that this reflects the same phenomena.[38]

One experimental result that might support this speculation is an experiment reported elsewhere.[39] A initial increase in PLT appears in alloy 4-4 directly after quenching from 540 ° C when aging took place at 0, −10 or −20 °C (p. 74 of ref. [39]. In this stage I, lower-temperature aging would induce a higher number density of clusters and shift the onset of saturated trapping to earlier aging times, thus revealing these clusters with a high intrinsic PLT.

A further notable point is the aging kinetics of samples quenched from different T_i during NA. Ideally, the NA kinetics should be proportional to the vacancy site fraction at the beginning of NA. However, we know that under some conditions, the kinetics are compressed, i.e., the kinetic differences are smaller than the (sometimes only indirectly inferred) differences in vacancy site fraction.[9,40]

A convenient measure for NA kinetics is the time T_{max} needed to reach the PLT maximum after interruption of the cooling process, which can be inverted to a rate T_{max}^{-1}. The maximum position is determined by polynomial fitting (see **Figure 7**a) for alloy 6014 and shown in Figure 7b as a function of the vacancy site fraction after interruption, i.e., at the beginning of NA, as calculated and shown in Figure 4c for 6014 and alloy 6-8-Sn. We notice an approximately linear relationship between the quantities for both the alloys, i.e., the rate of NA is approximately proportional to the vacancy site fraction, with possibly a slight deviation from linearity towards higher vacancy site fractions, which could indicate kinetic compression at higher temperatures. As we do not observe a PLT maximum above 400 °C (see Figure 2b), such compression cannot be verified with this method. The rate in alloy 6014 is about four times higher than in alloy 6-8-Sn, which we attribute to the presence of Sn.

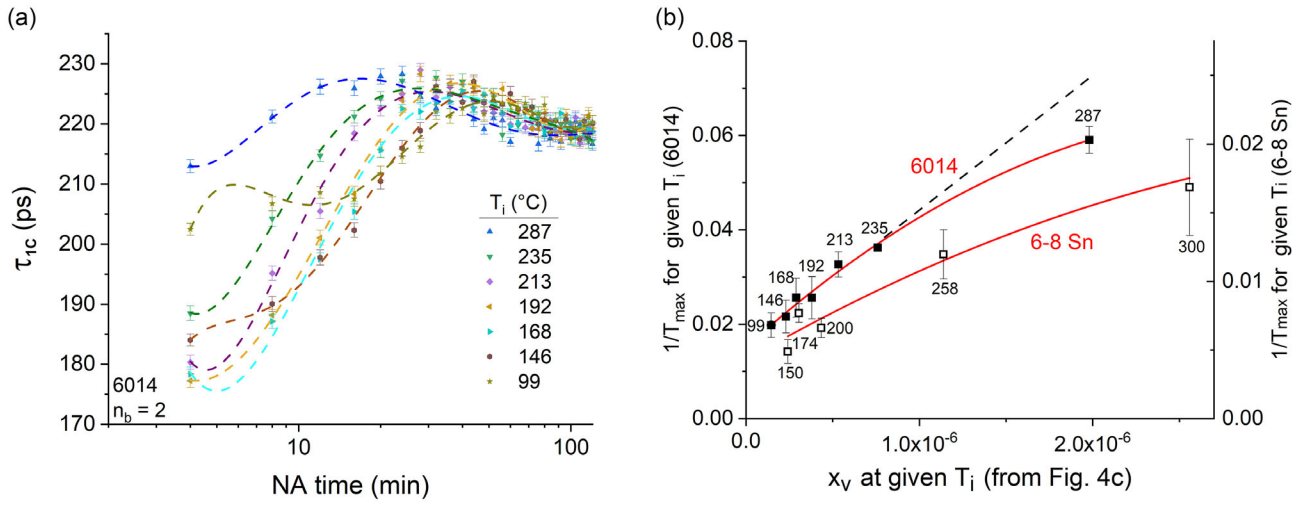

Figure 7. a) Evolution of τ_{1C} in alloy 6014 after solutionizing, cooling to T_i and quenching during ensuing NA. Curves from Figure 2b were selected that show a clear maximum after an initial increase. First 120 min of NA is shown. The curves are fitted by fifth-order polynomials to determine the times of the maximum T_{max}. b) The inverse of T_{max} is displayed vs. the calculated vacancy site fraction x_v after interrupting quenching at T_i that is read from Figure 4c. The labels give T_i. Data for alloy 6-8 Sn has been added for matters of comparison (right axis applies). The broken line is a linear extrapolation based on all except the data point for 287 °C.

4.4.3. Effect of Sn on NA Kinetics

In Section 3.2, we have seen an effect of Sn during air cooling. Here, we discuss that the addition of Sn also delays the kinetics of NA and the same mechanism can be accounted for, namely, trapping vacancies by Sn atoms. Two aspects are worth noting.

First, the effect of Sn depends on alloy composition. As it has been described earlier, the kinetic delay in 4-4 alloy caused by 45 at.ppm Sn is ≈100, whereas this factor is only ≈10 in 6-8 alloy with the same amount of added Sn. Such alloy dependence has been shown by Werinos et al.[41,42] and Liu et al.[11] and has been explained by the solubility of Sn at various Mg and Si contents.

Furthermore, the effect of Sn is also strong despite the rather low cooling rate. This is a little surprising as it is assumed that Sn binds Mg strongly[26] and would form precipitates during cooling which weakens the effect of Sn by lowering the dissolved Sn in the matrix, especially in 6-8 alloy where Mg and Si are both high. Such sensitivity to cooling has been shown in a 6061 alloy with Sn addition.[43] However, it is shown that the delaying effect of Sn is not influenced at all by first cooling to 200 °C (see Figure 2g). Thanks to the delay by Sn, stage I of alloy 6-8 can be now clearly distinguished in 6-8-Sn, which allows us to quantify the NA kinetics (see Figure 7b). The insensitivity of Sn to the cooling rate might be related to the absence of Fe and Mn in our alloys. These elements have low solubility in Al and therefore form intermetallic particles. Mg_2Sn phase was found to nucleate on the Al(Fe,Mn)Si particles[43] and lower the solubility of Sn. Therefore, engineering the Al(Fe,Mn)Si phase might help to prevent the loss of Sn and enlarge the cooling process window in Sn-modified alloys.

5. Conclusions

During air cooling from a solutionizing temperature of 540 °C at an initial rate of 8 K s^{-1}, PLT first decreases and then increases for all the ternary alloys investigated, while it continues to decrease for the binary alloy. This shows that during quenching, two mechanisms are active, continuous vacancy loss that reduces PLT and solute clustering that increases it at temperatures around 200 °C and below. Such clustering is found to be stronger for both higher Si and higher total solute content and is therefore weaker in the lean alloys. The addition of Sn delays the clustering process as known from isothermal aging experiments. The effect of Sn is most visible at low temperature and the effect is not impacted by slow cooling in the currently studied pure ternary alloys. Unlike solute clusters formed below 200 °C, an effect of the precipitates formed at higher temperatures during cooling (β′ and B′) is not visible in the PLT signal. Detection of the clustering signal below 200 °C has not been possible neither with DSC nor through electrical resistivity experiments, thus showing the added value of PLT measurements during cooling.

The PLT during NA after interrupted cooling to various T_i converges to a master kinetic curve for Al–Mg–Si alloys after a short time. The early NA stage in some of the Al–Mg–Si alloys might contain a hitherto undiscovered stage, in which solute clusters can contain excess open volume and increase PLT.

By interrupting a cooling process in various stages by fast quenching, one can therefore monitor the development of microstructure even with a "slow method" such as positron spectroscopy. By building suitable devices for thermal treatments of samples, one could apply this procedure to arbitrary heat treatments including quenching processes at faster rates than described here.

Appendix: Some Properties of Positron Annihilation

A.1 Positron Lifetime Contribution of Vacancy Clusters

The formation of divacancies or even larger vacancy clusters from individual vacancies might also increase PLT (+D, in Table 2). This can be shown using calculated values for the PLT τ_D in vacancy clusters of different sizes[44] and the corresponding trapping coefficients μ_D.[45] Using this data in the two-state trapping model,[14] we obtain the average PLT, which then includes annihilation in vacancy clusters and in the bulk.

The two-state trapping model allows one to calculate the intensities and lifetime components expected in a PLT spectrum, namely, I_i and τ_i, where $i = 1,2$. We use the notation that alpha-numerical indices (d, b) refer to the physical properties of the defect or the bulk, whereas numbers (1, 2) denote the two lifetime components measured in the spectrum.

From the given site fraction of the defect x_d and its trapping coefficient μ_d, the trapping rate κ_d is calculated

$$\kappa_d = \mu_d x_d \tag{A1}$$

We derive the components of the PLT spectrum

$$I_2 = \frac{\kappa_d}{{\tau_b}^{-1} + \kappa_d - {\tau_d}^{-1}} \tag{A2}$$

$$I_1 = 1 - I_2 \tag{A3}$$

$$\tau_2 = \tau_d \tag{A4}$$

$$\tau_1 = \frac{1}{{\tau_b}^{-1} + \kappa_d} \tag{A5}$$

$$\overline{\tau} = I_1\tau_1 + I_2\tau_2 \tag{A6}$$

where the PLTs for annihilation in the bulk and in a vacancy are $\tau_b = 160$ and $\tau_d = 245$ ps.

The latter equation can be written in a more compact form by inserting Equation (A1)–(A5) into Equation (A6). We obtain

$$\overline{\tau} = \tau_B \frac{1 + x_d\mu_d\tau_d}{1 + x_d\mu_d\tau_B} \tag{A7}$$

Figure A1a shows the calculated τ_D in vacancy clusters of different sizes as taken from different sources. In Figure A1b, the average PLT in an alloy containing a uniform distribution of clusters of a given size (including single vacancies) as calculated from Equation (A7) is given. The curves are based on three values for the single defect site fraction x_d directly after quenching and the assumption that all these vacancies are regrouped into vacancy clusters of a given size while preserving the number of

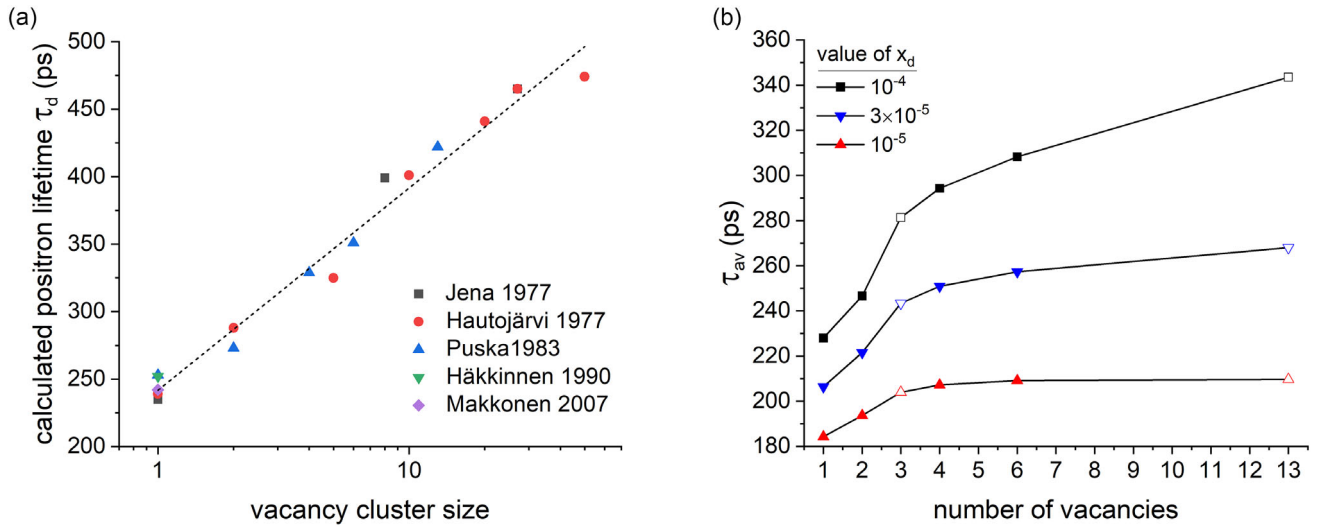

Figure A1. a) Calculated PLT in vacancy clusters of different sizes (in units of vacancy number). Various sources are compared.[44,46–49] Broken line is a linear fit to all the data on the logarithmic cluster size scale. b) Average PLT in Al containing a given site fraction x_d of vacancies (3 values) or the equivalent as vacancy clusters. Open symbols: defect lifetime or trapping coefficient was interpolated.

vacancies. The PLTs τ_d are from ref. [44], and trapping coefficients μ_d are taken from ref. [45]. The curves are all increasing, which is the consequence of a trapping coefficient that increases more rapidly with the size of the clusters than the specific PLT in such vacancy clusters and overcompensates the reduction of the number of trapping sites caused by the condensation of vacancies. Obviously, whenever a large number of vacancies condenses into divacancies, trivacancies or larger vacancy clusters, a notable increase of average and thus measured PLT will be observed.

A.2 Representing Average PLT by One-Component PLT

To assess the difference between an experimental PLT averaged over two measured components and a measured one-component lifetime, we carried out a simulation based on the two-state trapping model (2STM) given by Equation (A1)–(A6) and considered only single vacancies that were allowed to vary in site fraction from $x_d = 0$ to 2.75×10^{-4}. The two lifetime components arising from a given vacancy site fraction and the corresponding average PLT $\overline{\tau}_{av}^{2STM}$ are then calculated.

Program LTSim (written by J. Kansy) is used to calculate simulated "experimental" PLT spectra (i.e., containing noise and the influence of spectrometer resolution) corresponding to these two components, after which the spectra are analyzed with program LT9 to extract a "fitted" one-component lifetime τ_{1C}^{fit}. The difference between τ_{1C}^{fit} and $\overline{\tau}_{av}^{2STM}$ is given in **Figure A2**.

For $x_d = 0$, the difference is zero because the spectrum contains only the bulk component (point not shown due to log. scale). As the vacancy component starts to increase a difference is noted that increases rapidly to more than 14 ps, which is reached for a vacancy site fraction around 5×10^{-5} or an intensity of the vacancy component of 87%. The fit variance of the one-component fit is very high since the spectra do not fit a single exponential. For even higher vacancy site fractions, the difference decreases again along with the fit variance as the spectrum is now increasingly dominated by the vacancy contribution.

In summary, one can expect one-component fits of spectra containing a vacancy and a bulk component to yield slightly too high values. In the range of normally occurring vacancy site fractions (10^{-6} to 10^{-4}), the deviation is up to 14 ps. For example, instead of $\overline{\tau} = 230$ ps, one might measure $\tau_{1C} = 244$ ps. In the presence of a further PLT component, e.g., from solute clusters, simulations show that the difference is reduced.

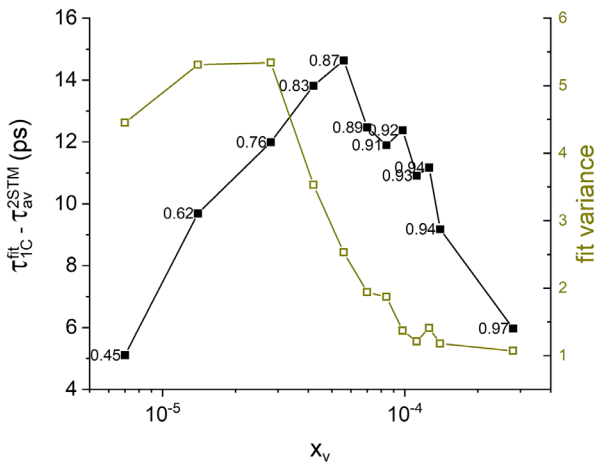

Figure A2. Difference between one-component τ_{1C}^{fit} and average PLT $\overline{\tau}_{av}^{2STM}$ in aluminum containing a varying site fraction of vacancies (full squares). The one-component lifetime was obtained by fitting a two-component spectrum with one component, which gives rise to an increased fit variance (open squares). The small labels are the intensities of the vacancy component I_v.

Table A1. Literature values for the properties of vacancies in Al (PLT τ_v and trapping coefficient μ_v) and of the PLT in the free matrix τ_b. Bottom line, values used in this article.

Authors	μ_v in s^{-1}	τ_b in ps	τ_v in ps	Ref.
Cotterill et al.	$2.3 \pm 0.5 \times 10^{14}\ s^{-1}$	166 ± 2	246 ± 2	[50]
Hall et. al	$3 \pm 2 \times 10^{14}\ s^{-1}$ at 473 K	$161 + 2$	243 ± 1	[51]
Hood et al.	$4.3 \times 10^{14}\ s^{-1}$ at 520 K	166		[52]
Fluss et al.	$4 \pm 1 \times 10^{14}\ s^{-1}$	166	244	[53]
Nieminnen et al.	$2.5 \times 10^{14}\ s^{-1}$ (calculated)	–	–	[45]
Jackman et al./Gramsch et al.	$2.5/2.4 \times 10^{14}\ s^{-1}$ at 200 K (only analysis)			[15]/[21]
Schäfer et al.	$4.5 \times 10^{14}\ s^{-1}$ at 715 K $1.1 \pm 0.5 \times 10^{15}\ s^{-1}$ at 120 K	$163 + 3$	$251 + 3$	[20] [20]
Elsayed et al.	$1.5 \times 10^{15}\ s^{-1}$	158	234 (with In)	[54]
This work	$2.5 \times 10^{14}\ s^{-1}$	160	245	–

A.3 Sensitivity of Average Positron Lifetime to Changes of Vacancy Site Fraction

Equation (A7) provides a relationship between the average PLT $\bar{\tau}$ and defect site fraction x_v. Inverting the relation allows us to calculate the vacancy site fraction needed to give rise to a given average PLT. We observe that for PLTs around 160 ps, the vacancy site fraction cannot be determined accurately due the high slope of the curve (range of "low sensitivity"). The same would formally apply to high PLTs, but these cannot appear in our experiments with a maximum solutionizing temperature of 540 °C (shaded area near right axis).

A crucial value is the trapping coefficient for vacancies in Al. We use a value given by Jackman.[15] However, μ is not known very precisely. Other values quoted in the literature are given in **Table A1**. Although there is a preference for values around $\mu_v = 2.5 \times 10^{14}\ s^{-1}$, higher values cannot completely be ruled out, which is why **Figure A3** also contains a calculation based on the highest value claimed in the literature, which would imply about ten times lower vacancy site fractions for the same average PLTs. The difficulty in determining precise values for x_v has two reasons: 1) In the more concentrated Al–Mg–Si alloys 6-8 and 6014, reliable decompositions of measured data into two components has not been possible. Only alloy 4-4 allows for such decompositions.[8] We therefore use the one-component lifetime τ_{1C} as a subsitute, which, however, can be higher than the average PLT (see Appendix A.2). 2) We do not know the exact vacancy site fraction after quenching from the solutionizing temperature and the influence of other positron traps such as solute clustering.

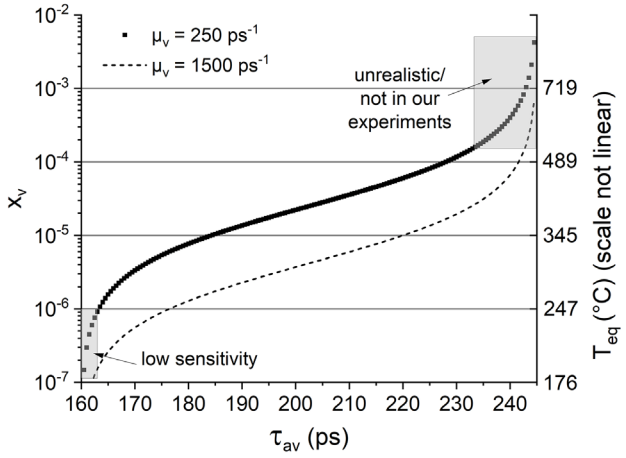

Figure A3. Vacancy site fraction corresponding to a given measured average PLT in Al with vacancies as the only defect. Full symbols reflect values used in this work for the discussion. Values are given in steps of 0.5 ps. Dotted line represents a six times higher alternative value of the trapping coefficient.[54] Right axis: temperature required to reach a given vacancy site fraction on the left axis by thermal treatment assuming a vacancy formation energy of 0.65 eV.

Acknowledgements

The authors thank Hydro Aluminium Bonn and Novelis Sierre for providing the alloy samples. There was no external funding for this work.

Open Access funding enabled and organized by Projekt DEAL.

Conflict of Interest

The authors declare no conflict of interest.

Data Availability Statement

The data that support the findings of this study are available from the corresponding author upon reasonable request.

Keywords

age-hardening, aluminum alloy, positron lifetime, vacancy

Received: July 30, 2025
Revised: November 10, 2025
Published online: December 12, 2025

[1] Y. Nagai, K. Takadate, Z. Tang, H. Ohkubo, H. Sunaga, H. Takizawa, M. Hasegawa, *Phys. Rev. B* **2003**, *67*, 224202.

[2] S. K. Sarkar, P. Maheshwari, P. K. Pujari, A. Biswas, *Acta Mater.* **2024**, *268*, 119740.

[3] R. Domínguez-Reyes, M. A. Monge, B. Galiana, Y. Ortega, A. Muñoz, G. Carro-Sevillano, *J. Alloys Compd.* **2022**, *900*, 163430.
[4] M. Liu, P. Diercks, A. Manzoni, J. Cižek, U. Ramamurty, J. Banhart, *Acta Mater.* **2021**, *220*, 117298.
[5] A. Dupasquier, G. Kogel, A. Somoza, *Acta Mater.* **2004**, *52*, 4707.
[6] A. Dupasquier, R. Ferragut, M. M. Iglesias, C. E. Macchi, M. Massazza, P. Mengucci, G. Riontino, A. Somoza, Positron Annihilation, Icpa-13, Proceedings **2004**, *445–456*, 16.
[7] J. Banhart, C. S. T. Chang, Z. Q. Liang, N. Wanderka, M. D. H. Lay, A. J. Hill, *Adv. Eng. Mater.* **2010**, *12*, 559.
[8] M. Liu, J. Čížek, C. S. T. Chang, J. Banhart, *Acta Mater.* **2015**, *91*, 355.
[9] Z. Yang, X. H. Jiang, X.-P. Zhang, M. Liu, Z. Q. Liang, D. Leyvraz, J. Banhart, *Scr. Mater.* **2021**, *190*, 179.
[10] J. Banhart, M. D. H. Lay, C. S. T. Chang, A. J. Hill, *Phys. Rev. B* **2011**, *83*, 014101.
[11] M. Liu, X. P. Zhang, B. Körner, M. Elsayed, Z. Q. Liang, D. Leyvraz, J. Banhart, *Materialia* **2019**, *6*, 100261.
[12] M. Madanat, M. Liu, X.-P. Zhang, Q.-N. Guo, J. Cizek, J. Banhart, *Phys. Rev. Mater.* **2020**, *4*, 063608.
[13] F. D. Fischer, J. Svoboda, F. Appel, E. Kozeschnik, *Acta Mater.* **2011**, *59*, 3463.
[14] R. Krause-Rehberg, *Positron Annihilation in Semiconductors*, Springer, Heidelberg **1999**.
[15] J. A. Jackman, G. M. Hood, R. J. Schultz, *J. Phys. F: Met. Phys.* **1987**, *17*, 1817.
[16] M. Liu, B. Klobes, J. Banhart, *J. Mater. Sci.* **2016**, *51*, 7754.
[17] J. Banhart, Z. Yang, Q. N. Guo, M. Liu, M. Butterling, M. O. Liedke, E. Hirschmann, A. Wagner, *Adv. Eng. Mater.* **2023**, *26*, 2300490.
[18] X. Z. Wang, D. D. Zhao, Y. J. Xu, Y. J. Li, *Acta Mater.* **2024**, *264*, 119552.
[19] J. L. Murray, *Bull. Alloy Phase Diagrams* **1982**, *3*, 60.
[20] H. E. Schaefer, R. Gugelmeier, M. Schmolz, A. Seeger, *Mater. Sci. Forum* **1987**, *15–18*, 111.
[21] E. Gramsch, K. G. Lynn, *Phys. Rev. B* **1989**, *40*, 2537.
[22] B. Milkereit, N. Wanderka, C. Schick, O. Kessler, *Mater. Sci. Eng. A* **2012**, *550*, 87.
[23] Z. Yang, X. H. Jiang, X. P. Zhang, M. Liu, Z. Liang, D. Leyvraz, J. Banhart, *MATEC Web Conf.* **2020**, *326*, 02005.
[24] Y. Yan, PhD thesis, Technische Universität Berlin **2014**, https://doi.org/10.14279/depositonce-4020.
[25] Z. Yang, S. Mallow, J. Banhart, O. Kessler, *Thermochim. Acta* **2024**, *739*, 179815.
[26] J. Peng, S. Bahl, A. Shyam, J. A. Haynes, D. W. Shin, *Acta Mater.* **2020**, *196*, 747.
[27] S. Pogatscher, H. Antrekowitsch, M. Werinos, F. Moszner, S. S. A. Gerstl, M. F. Francis, W. A. Curtin, J. F. Löffler, P. J. Uggowitzer, *Phys. Rev. Lett.* **2014**, *112*, 225701.
[28] M. Liu, J. Čižek, C. S. T. Chang, J. Banhart, *Mater. Sci. Forum* **2014**, *794–796*, 33.
[29] M. Liu, Q. Guo, X. Zhang, M. Wüstenhagen, J. Čížek, J. Banhart, *Scr. Mater.* **2020**, *177*, 203.
[30] C. Wolverton, *Acta Mater.* **2007**, *55*, 5867.
[31] S. Hirosawa, F. Nakamura, T. Sato, *Mater. Sci. Forum* **2007**, *561–565*, 283.
[32] P. Lang, E. Povoden-Karadeniz, W. Mayer, A. Falahati, E. Kozeschnik, in *8th Pacific Rim International Conference on Advanced Materials and Processing*, (Ed: F. Marquis), Wiley, Hoboken, NJ **2013**, pp. 3181.
[33] T. Saito, E. A. Mortsell, S. Wenner, C. D. Marioara, S. J. Andersen, J. Friis, K. Matsuda, R. Holmestad, *Adv. Eng. Mater.* **2018**, *20*, 1800125.
[34] O. I. Gorbatov, A. Y. Stroev, Y. N. Gornostyrev, P. A. Korzhavyi, *Acta Mater.* **2019**, *179*, 70.
[35] M. Mizuno, K. Sugita, H. Araki, *Materialia* **2020**, *13*, 100853.
[36] S. Q. Zhu, H. C. Shih, X. Y. Cui, C. Y. Yu, S. P. Ringer, *Acta Mater.* **2021**, *203*, 116455.
[37] K. Strobel, M. D. H. Lay, M. A. Easton, L. Sweet, S. M. Zhu, N. C. Parson, A. J. Hill, *Mater. Charact.* **2016**, *111*, 43.
[38] M. A. Madanat, PhD thesis, Technische Universität **2018**. https://doi.org/10.14279/depositonce-7112.
[39] M. Liu, PhD thesis, Technische Universität Berlin **2014**. https://doi.org/10.14279/depositonce-4207.
[40] Z. Yang, Z. Q. Liang, D. Leyvraz, J. Banhart, *Materialia* **2019**, *7*, 100413.
[41] M. Werinos, H. Antrekowitsch, T. Ebner, R. Prillhofer, P. J. Uggowitzer, S. Pogatscher, *Mater. Des.* **2016**, *107*, 257.
[42] M. Werinos, H. Antrekowitsch, T. Ebner, R. Prillhofer, W. A. Curtin, P. J. Uggowitzer, S. Pogatscher, *Acta Mater.* **2016**, *118*, 296.
[43] F. Schmid, P. J. Uggowitzer, R. Schäublin, M. Werinos, T. Ebner, S. Pogatscher, *Materials* **2019**, *12*, 1801.
[44] M. Puska, R. M. Nieminen, *J. Phys. F: Met. Phys.* **1983**, *13*, 333.
[45] R. M. Nieminen, J. Laakkonen, *Appl. Phys.* **1979**, *20*, 181.
[46] P. Jena, A. K. Gupta, K. S. Singwi, *Solid State Commun.* **1977**, *21*, 293.
[47] P. Hautojärvi, J. Heiniö, M. Manninen, *Philos. Mag.* **1977**, *35*, 973.
[48] H. Häkkinen, S. Mäkinen, M. Manninen, *Phys. Rev. B* **1990**, *41*, 12441.
[49] I. Makkonen, M. J. Puska, *Phys. Rev. B* **2007**, *76*, 054119.
[50] R. M. J. Cotterill, K. Petersen, G. Trumpy, G. Träff, *Journal of Physics F* **1972**, *2*, 459.
[51] T. M. Hall, A. N. Goland, T. L. Snead, *Phys. Rev. B* **1974**, *10*, 3062.
[52] G. M. Hood, B. T. A. Mckee, *J. Phys. F-Met. Phys.* **1978**, *8*, 1457.
[53] M. J. Fluss, L. C. Smedskjaer, M. K. Chason, D. G. Legnini, R. W. Siegel, *Phys. Rev. B* **1978**, *17*, 3444.
[54] M. Elsayed, T. E. M. Staab, J. Cizek, R. Krause-Rehberg, *Acta Mater.* **2021**, *219*, 117228.

